Novel Fe_3O_4@SiO_2@Ag@Ni trepang-like nanocomposites: High-efficiency and magnetic recyclable catalysts for organic dye degradation*

Chao Li(李超), Jun-Jie Sun(孙俊杰), Duo Chen(陈铎), Guang-Bing Han(韩广兵), Shu-Yun Yu(于淑云), Shi-Shou Kang(康仕寿)†, and Liang-Mo Mei(梅良模)

School of Physics and National Key Laboratory of Crystal Materials, Shandong University, Jinan 250100, *China*

(Received 13 January 2016; revised manuscript received 17 April 2016; published online 25 June 2016)

A facile step-by-step approach is developed for synthesizing the high-efficiency and magnetic recyclable Fe_3O_4@SiO_2@Ag@Ni trepang-like nanocomposites. This method involves coating Fe_2O_3 nanorods with a uniform silica layer, reduction in 10% H_2/Ar atmosphere to transform the Fe_2O_3 into magnetic Fe_3O_4, and finally depositing Ag@Ni core-shell nanoparticles on the L-lysine modified surface of Fe_3O_4@SiO_2 nanorods. The fabricated nanocomposites are further characterized by x-ray diffraction, transmission electron microscopy, scanning electron microscope, Fourier transform infrared spectroscopy, and inductively coupled plasma mass spectroscopy. The Fe_3O_4@SiO_2@Ag@Ni trepang-like nanocomposites exhibit remarkably higher catalytic efficiency than monometallic Fe_3O_4@SiO_2@Ag nanocomposites toward the degradation of Rhodamine B (RhB) at room temperature, and maintain superior catalytic activity even after six cycles. In addition, these samples could be easily separated from the catalytic system by an external magnet and reused, which shows great potential applications in treating waste water.

Keywords: trepang-like nanocomposites, core-shell nanoparticles, catalytic property, magnetic property

PACS: 82.65.+r, 81.20.–n, 68.43.–h **DOI:** 10.1088/1674-1056/25/8/088201

1. Introduction

Noble metal (e.g., Pt, Au, Pd, Ag) nanostructures have received considerable attention due to their unique physical and chemical properties, as well as their excellent performance in optical devices,[1] catalysts,[2] fuel cell,[3] and sensors.[4] Especially in the field of water treatment, degradation of organic dye by using noble metal based catalysts has become one of the topics of great interest due to their high activities and efficiencies.[5–8] However, high cost and scarce resources restrict the further applications of the noble metals in practical industry. To solve these problems, recent researches have focused on partially replacing noble metals by other non-noble materials, such as transition metals (Fe, Co, Ni, Cu). Zhang *et al.* synthesized Ag/Cu@Fe_3O_4 bimetallic nanoparticles by the co-reduction method, and the as-prepared samples showed superior catalytic activity for the reduction of 4-nitrophenol.[9] Dhanda and Kidwai reported the syntheses and characterizations of the reduced graphene oxide supported Ag_xNi_{100-x} alloy nanoparticles which exhibit highly catalystic efficiency for p-nitrophenol reduction.[10] Zhang *et al.* designed uniform Ni/SiO_2@Au hollow microspheres and these bimetallic nanocomposites displayed a better catalytic performance than monometallic SiO_2@Au microspheres in 4-nitrophenol reduction experiment.[11] It was reported that core–shell nanoparticles are often found to be catalytically more active than their monometallic counterparts and alloy due to the electronic and lattice effects between the adjacent metals.[12,13] Unfortunately, little attention has been paid to synthesizing the bimetallic core-shell nanocomposites which are constructed with noble and non-noble metals, and to investigating their catalytic activities for the degradation of organic dye either.[14]

Metal nanoparticles often suffer aggregation and leaching without protection or surface passivation, owing to their high surface energies. This will lead to fast reducing the catalytic activity and stability. A solving method is normally to immobilize and graft the metal nanoparticles onto inorganic supports, such as polystyrene silica,[15] carbon,[16] and magnetic microspheres.[17,18] Among these catalyst supports, magnetic iron oxide nanoparticles coated with a silica layer are often employed because of their relatively high saturation magnetization, and could be easily recovered by using an external magnetic field.[19–21] The SiO_2 shell can not only protect the magnetic core from being corroded but also supply a suitable supporting matrix to incorporate other functional materials. On the other hand, it was believed that the shape of the nanoparticles could greatly affect the catalytic activity for a heterogeneous catalyst system, in which particles with high aspect ratio show higher diffusion and catalytic rate than particles with low aspect ratio.[22–26] Thus, it is also important to

*Project supported by the National Basic Research Program of China (Grant No. 2015CB921502), the National Natural Science Foundation of China (Grant Nos. 11474184 and 11174183), the 111 Project (Grant No. B13029), and the Fundamental Research Funds of Shandong University, China.

†Corresponding author. E-mail: skang@sdu.edu.cn

© 2016 Chinese Physical Society and IOP Publishing Ltd

select magnetic supports with suitable morphology.

In this work, we develop a simple method of preparing the Fe_3O_4@SiO_2@Ag@Ni trepang-like hybrid nanostructure. As depicted in Fig. 1, Fe_2O_3 nanorods are first synthesized and coated with a SiO_2 shell by the hydrolysis and condensation of TEOS. After being calcined at 450 °C in a reduction atmosphere, the Fe_3O_4@SiO_2 nanorods are modified with L-lysine and then Ag@Ni core-shell nanoparticles are deposited on the surface of Fe_3O_4@SiO_2 nanorods through a one-pot reduction reaction. It is found that the fabricated Fe_3O_4@SiO_2@Ag@Ni trepang-like nanocomposites show a remarkably catalytic ability for the degradation of RhB by $NaBH_4$.

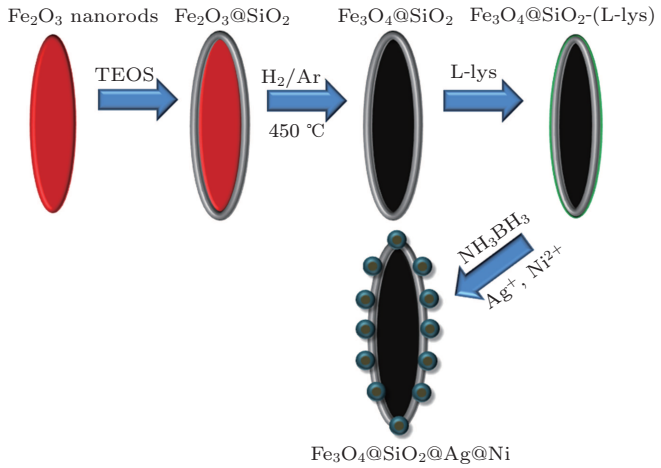


Fig. 1. (color online) Synthetic procedure of the Fe_3O_4@SiO_2@Ag@Ni trepang-like nanocomposites.

2. Experiment

2.1. Materials

L-lysine, ferric chloride ($FeCl_3{\cdot}6H_2O$), nickel nitrate ($Ni(NO_3)_2{\cdot}6H_2O$), silver nitrate ($AgNO_3$), ammonium dihydrogen phosphate ($NH_4H_2PO_4$), ammonia hydroxide (25 wt%), tetraethyl orthosilicate (TEOS), sodium borohydride ($NaBH_4$ 98%), and Rhodamine B were purchased from Aladdin, and ammonia borane (NH_3BH_3 90%) was purchased from Aldrich. All of them were directly used without further purification.

2.2. Synthesis of Fe_2O_3@SiO_2 nanorods

Monodispersed Fe_2O_3 nanorods were fabricated through a modified hydrothermal method previously reported.[27] Typically, 0.8 mmol of $FeCl_3{\cdot}6H_2O$ and 0.3×10^{-5} mmol of $NH_4H_2PO_4$ were dissolved in 40-mL deionized water and stirred for 15 min. After that, the solution was transferred into a 50-mL Teflon-lined stainless-steel autoclave and aged at 220 °C for 40 h. When the autoclave cooled to room temperature, the precipitates were centrifuged and washed with deionized water three times. For coating Fe_2O_3 nanorods with a silica layer, particles were dispersed into a solution containing water (20 mL), absolute ethanol (160 mL), and TEOS (60 μL). The mixture was sonicated for 15 min, then 3-mL ammonia hydroxide solution was added into the mixture drop by drop. After stirring at room temperature for 6 h, the products were washed with ethanol and dried at 50 °C for 12 h.

2.3. Syntheses of Fe_3O_4@SiO_2 nanorods

To convert the obtained Fe_2O_3@SiO_2 nanorods into magnetic Fe_3O_4@SiO_2 nanorods, the sample was calcined at 450 °C in 10% H_2/Ar atmosphere for 6 h.

2.4. Syntheses of Fe_3O_4@SiO_2@Ag@Ni trepang-like nanocomposites

50-mg Fe_3O_4@SiO_2 nanorods and 300-mg L-lysine were added into 50-mL deionized water and sonicated for 60 min. The products were washed with deionized water three times and transferred into a three-neck round-bottom flask containing 30-mL deionized water, then 1-mL $Ni(NO_3)_2$ solution (0.02 M) and 1-mL $AgNO_3$ solution (0.02 M) were added. After stirring for 60 min, 4-mL ammonia borane solution (0.5 M) was dropped into the mixture slowly and sonicated for another 30 min under N_2 atmosphere. The products were collected by a magnet, purified with deionized water and dried at 50 °C for 6 h. Fe_3O_4@SiO_2@Ag nanocomposites were also fabricated in a similar way by adding 0.04-mmol $AgNO_3$ precursors and without the addition of $Ni(NO_3)_2$.

2.5. Catalytic degradation of Rhodamine B

The catalytic activity of the fabricated sample was tested by using the degradation of Rhodamine B as a model reaction. Typically, 1-mL $NaBH_4$ aqueous solution (0.1 M) was added into a 50-mL beaker containing 20 mL of RhB aqueous solution (5×10^{-5} M). Then, 1-mL aqueous dispersion of the Fe_3O_4@SiO_2@Ag nanocomposites (5 mg·mL^{-1}) was dropped into the above solution. A 2-mL mixture was taken out every 3 min and the UV-Vis absorption peak at 553 nm was recorded at room temperature. A similar procedure was used for testing the catalytic activities of Fe_3O_4@SiO_2@Ag nanocomposites and Fe_3O_4@SiO_2 nanorods.

2.6. Characterization

The crystalline structure was investigated by x-ray power diffraction (Bruker D8 ADVANCE). The transmission electron microscopy (TEM), high-resolution transmission electron microscopy (HRTEM) were conducted on a JEM 1200EX microscope operated at 200 kV. The SEM photographs and element analysis were conducted on an S-4800 scanning electron microscope. The Fourier transform infrared spectra (FT-IR) of the samples were measured with a NEXUS 670 FT-IR spectrometer. The ultraviolet-visible (UV-vis) spectrum measurements were recorded on an F-4500 ultraviolet-visible spectrophotometer. The magnetic properties of the products were measured by an alternative gradient magnetometer

(2900-04C). The inductively coupled plasma mass spectrum (ICP-MS) was measured by using an Agilent 7500ce system.

3. Results and discussion

The phase and crystalline composition of the as-prepared samples are examined by XRD measurements. Figure 2(a) is a typical XRD pattern of the Fe_2O_3 nanorods. Compared with the data in JCPDS 87-1165, all the diffraction peaks can be indexed to trigonal α-Fe_2O_3. After annealing treatment in H_2/Ar flow, the phase is completely transformed into cubic Fe_3O_4 (JCPDS75-1609) (Fig. 2 (curve *b*)). Figure 2 (curve *c*) shows the XRD pattern of the Fe_3O_4@SiO_2@Ag@Ni trepang-like nanocomposites, and it is clearly seen that besides the characteristic peaks of Fe_3O_4, the obvious diffraction peaks at $2\theta = 38.2°$, 44.4°, 64.6°, and 77.5° can be readily indexed to the (111), (200), (220), and (311) crystal planes of metallic Ag (JCPDS No. 87-0720), no other diffraction peaks can be observed in the XRD pattern, suggesting amorphous characters of Ni and SiO_2.

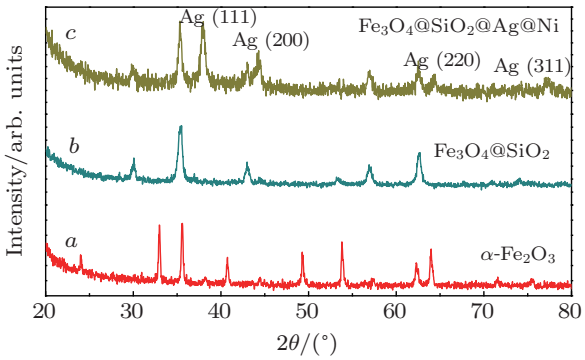


Fig. 2. (color online) XRD patterns of the synthesized (a) Fe_2O_3 nanorods, (b) Fe_3O_4@SiO_2 nanorods, and (c) Fe_3O_4@SiO_2@Ag@Ni trepang-like nanocomposites.

Figure 3 shows the TEM images of Fe_2O_3 nanorods, Fe_2O_3@SiO_2 nanorods and Fe_3O_4@SiO_2 nanorods respectively. As shown in Fig. 3(a), the average length and diameter of the Fe_2O_3 nanorods are about 450 nm and 90 nm, respectively. After being coated with the SiO_2 layer, the Fe_2O_3@SiO_2 nanorods exhibit a typical core-shell structure (Fig. 3(b)). The TEM image inset in Fig. 3(b) clearly reveals that the Fe_2O_3 nanorod is encapsulated in a gray SiO_2 film whose overall thickness is about 10 nm. The subsequent thermal transformation process did not destroy the rod shape of the obtained Fe_3O_4@SiO_2 (Fig. 3(c)), which may be due to the presence of the SiO_2 shell. Figure 3(d) shows the HRTEM image of Fe_3O_4@SiO_2 nanorods, and the d-spacing of the crystallized part is about 0.294 nm, which is consistent with the (220) plane in cubic magnetite crystal.

In order to facilitate the attachments of Ag^+, Ni^{2+} ions, the surfaces of the Fe_3O_4@SiO_2 nanorods are modified with L-lysine. Figure 4 shows the FTIR spectrum of the L-lysine modified Fe_3O_4@SiO_2 nanorods. Fe_3O_4 displays a typical absorption peak at 575 cm^{-1} which corresponds to Fe–O stretching vibration. The peak at 1094 cm^{-1} can be assigned to the asymmetric stretching vibration of Si–O–Si, indicating that SiO_2 is coated on the surfaces of Fe_3O_4 nanorods. The peak at 3431 cm^{-1} due to (–OH) stretching vibrations can be attributed to the hydroxyls adsorbed on the surface of the SiO_2 shell. The peaks at 1629 cm^{-1} and 2920 cm^{-1} can be attributed to –N–H– in-plan bending vibrations and –C–H stretching vibrations respectively,[9,28] which confirms that the L-lysine is successfully bound to the surfaces of Fe_3O_4@SiO_2 nanorods.

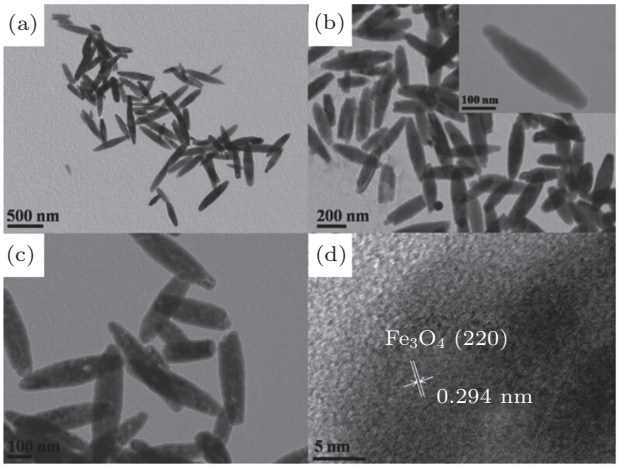


Fig. 3. TEM images of the as-synthesized (a) Fe_2O_3 nanorods, (b) Fe_2O_3@SiO_2 nanorods, (c) Fe_3O_4@SiO_2 nanorods; (d) HRTEM image of Fe_3O_4@SiO_2 nanorods.

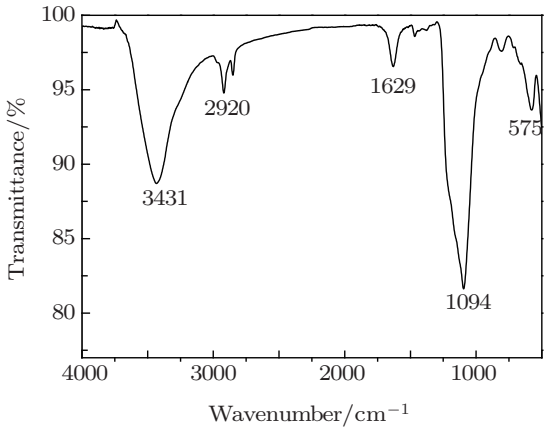


Fig. 4. FTIR spectra of L-lysine modified Fe_3O_4@SiO_2 nanorods.

In the synthesis of Fe_3O_4@SiO_2@Ag@Ni trepang-like nanocomposites, NH_3BH_3 was used as the reducing agent. It is known that Ni^{2+} cannot be directly reduced by NH_3BH_3 because of the low reduction potential (E^0 (Ni^{2+} + /Ni) = −0.25 eV versus SHE). So the Ag^+ is reduced first by NH_3BH_3 due to its high reduction potential (E^0 (Ag^+/Ag) = +0.80 eV versus SHE) and Ag nanoparticles are formed on the surfaces of Fe_3O_4@SiO_2 nanorods, serving as seeds to induce the subsequent growths of Ni nanoparticles due to the excellent reducing activity of Ag–H species.[29] Finally

the Fe_3O_4@SiO_2@Ag@Ni trepang-like nanocomposites are obtained.

The SEM images of the Fe_3O_4@SiO_2@Ag@Ni trepang-like nanocomposites obtained at different magnifications are displayed in Fig. 5. Figure 5(a)–5(b) illustrate that the trepang-like nanocomposites whose lengths are in a range of 450 nm–550 nm and widths are in a range of 120 nm–140 nm, are uniformly synthesized. This high magnification SEM image in Fig. 5(c) reveals that monodispersed Ag nanoparticles and Ni nanoplatelets are successfully coated around the Fe_3O_4@SiO_2 nanorods. EDS analysis (Fig. 5(d)) and area mapping (Fig. 6) of the sample confirm that the multicomponent composite consists of Fe, Ag, Ni, Si, C, and O. The strong Si peak in Fig. 5(d) is mainly due to the Si substrate, and the C element may come from the L-lysine. The actual elemental composition and percentage loading of Fe_3O_4@SiO_2@Ag nanorods and Fe_3O_4@SiO_2@Ag@Ni trepang-like nanocomposites are further analyzed by the ICP-MS study. The results suggest that the content of Ag is about 0.86 mmol in per gram of the Fe_3O_4@SiO_2@Ag nanocomposites, the content values of Ag and Ni are about 0.50 mmol and 0.44 mmol in per gram of the Fe_3O_4@SiO_2@Ag@Ni trepang-like nanocomposites, which are near to the initial precursor percentages.

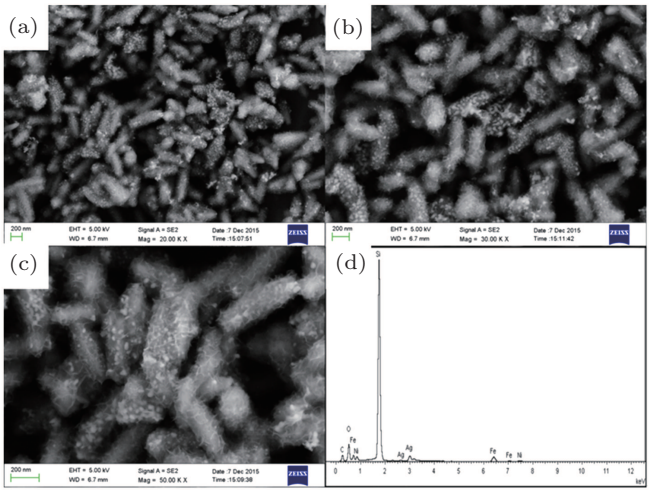


Fig. 5. (color online) (a)–(c) Scanning electron microscope images of the Fe_3O_4@SiO_2@Ag@Ni trepang-like nanocomposites with different magnifications; (d) EDS spectrum of the Fe_3O_4@SiO_2@Ag@Ni trepang-like nanocomposites.

The morphologies and structures of the Fe_3O_4@SiO_2@Ag@Ni trepang-like nanocomposites are further investigated by TEM and HRTEM. TEM images in Fig. 7 clearly show that the black Ag nanoparticles are well-dispersed on Fe_3O_4@SiO_2 nanorods with the size ranging from 10 nm to 20 nm, and coated with a gray Ni layer whose thickness is about 20 nm, which is consistent with the SEM result. Compared with the Fe_3O_4@SiO_2 nanorods shown in Fig. 3, the sizes of Fe_3O_4@SiO_2@Ag@Ni trepang-like nanocomposites are up to 550 nm in length and 140 nm in width. The interplanar distance of the crystallized core part is 0.236 nm (Fig. 7(d)), which is consistent with the Ag (111). No crystalline lattice is observed in the thin gray slices, indicating the disorder nature of the Ni layer, which is in agreement with the XRD result.

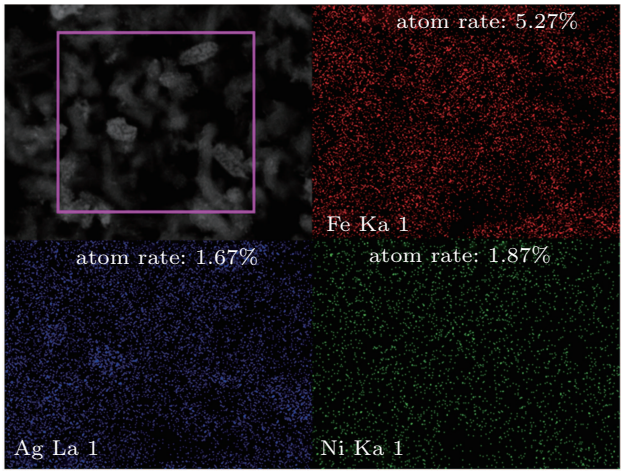


Fig. 6. (color online) Area mapping of the Fe_3O_4@SiO_2@Ag@Ni trepang-like nanocomposites.

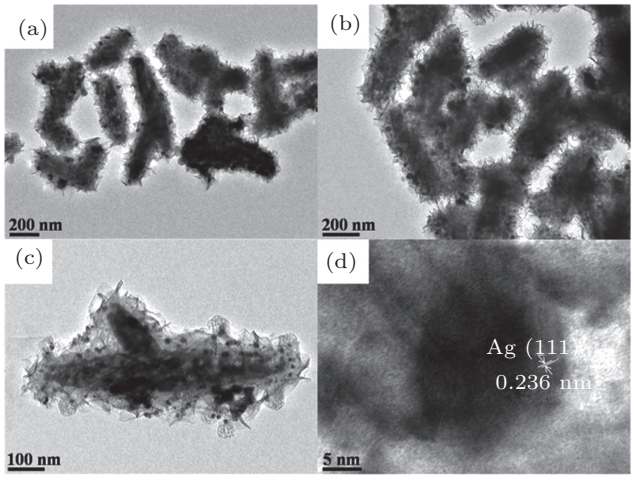


Fig. 7. (a)–(c) TEM images of Fe_3O_4@SiO_2@Ag@Ni trepang-like nanocomposites with different magnifications; (d) HRTEM image of Ag nanoparticle.

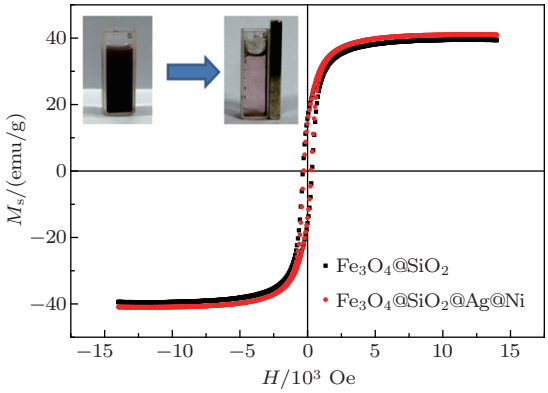


Fig. 8. (color online) Magnetization curves measured at room temperature for Fe_3O_4@SiO_2 nanorods (black), and Fe_3O_4@SiO_2@Ag@Ni trepang-like nanocomposites (red). The unit 1 Oe = 79.5775 A·cm^{-1}.

The hysteresis loops of the Fe_3O_4@SiO_2 nanorods and Fe_3O_4@SiO_2@Ag@Ni trepang-like nanocomposites are

measured by an AGM instrument at the room temperature. As shown in Fig. 8, both of the samples exhibit a typical ferromagnetic behavior. The M_s value of the Fe_3O_4@SiO_2@Ag@Ni trepang-like nanocomposites (41.2 emu·g^{-1}) is higher than that of Fe_3O_4@SiO_2 nanorods (39.5 emu·g^{-1}), which can be attributed to the magnetic nickel metal shell. The coercivity values of the Fe_3O_4@SiO_2 nanorods (338 Oe, 1 Oe = 79.5775 A·m^{-1}) and Fe_3O_4@SiO_2@Ag@Ni trepang-like nanocomposites (297 Oe) are much higher than that of Fe_3O_4 nanoparticles reported previously,[30,31] which may come from the enhanced shape anisotropy.[32] These catalysts could be easily collected by an external magnet (inset in Fig. 8) after the degradation reaction, which is facilitative for the recycle applications.

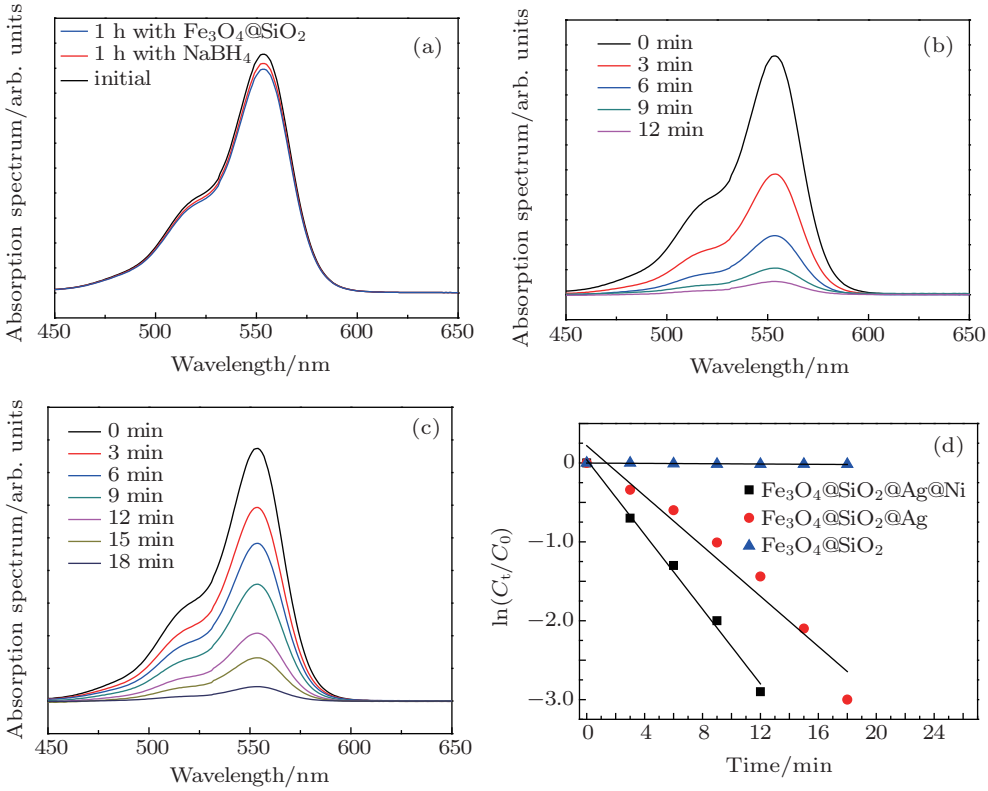


Fig. 9. (color online) UV-Vis absorption spectra for the reduction of RhB by $NaBH_4$ in the presence of (a) Fe_3O_4@SiO_2 nanorods, (b) Fe_3O_4@SiO_2@Ag@Ni trepang-like nanocomposites, and (c) Fe_3O_4@SiO_2@Ag nanorods; (d) plots of ln (C_t/C_0) versus time for rate constant calculation of the as-synthesized samples.

Degradation of RhB in the presence of $NaBH_4$ is chosen as a model reaction to evaluate the catalytic activities of the products. Figure 9 shows the UV-Vis absorption spectra for the reduction of RhB by $NaBH_4$ in the presence of Fe_3O_4@SiO_2 nanorods, Fe_3O_4@SiO_2@Ag@Ni trepang-like nanocomposites, and Fe_3O_4@SiO_2@Ag nanocomposites. Nearly no intensity change of the peak at 553 nm is found after 1 h reaction (Fig. 9(a)), indicating that the reduction is very slow without the catalysts. After adding the catalysts, the absorption peak at 553 nm gradually decreases with the reaction time increasing. It took about 12 min and 18 min for the Fe_3O_4@SiO_2@Ag@Ni trepang-like nanocomposites (Fig. 9(b)) and Fe_3O_4@SiO_2@Ag nanocomposites (Fig. 9(c)) to complete the catalytic reaction respectively. The linear variation of $\ln(C_t/C_0)$ with reaction time shows that these reactions follow the first-pseudo-order kinetics[33] (Fig. 9(d)), where the C_0 and C_t represent the concentrations of RhB after time 0 and t min respectively. According to the formula

$$\ln(C_t/C_0) = -kt,$$

the values of apparent rate constant k estimated from the slopes of the straight lines are 0.23 min^{-1}, 0.15 min^{-1}, and 0.0015 min^{-1} for the Fe_3O_4@SiO_2@Ag@Ni trepang-like nanocomposites, Fe_3O_4@ SiO_2@Ag nanocomposites, and Fe_3O_4@SiO_2 nanorods, respectively. Fe_3O_4@SiO@Ag@Ni trepang-like nanocomposites exhibit a higher catalytic activity than the monometallic Fe_3O_4@SiO_2@Ag nanocomposites, which may be due to the reasons as follows. (i) As is well known, the catalytic activities of the metal particles come from their ability to transfer electrons from donor to acceptor.[34,35] The SEM and TEM images shown in Figs. 5 and 7 have revealed that the Fe_3O_4@SiO_2@Ag@Ni trepang-like nanocomposites provide large specific surface areas, owing to their unique morphologies, which are favorable for adsorbing the reducing agents and dye molecules to the surface of the catalyst and facilitating the catalytic degradation. (ii) The electronic structure (d band) of the Ag@Ni core-shell nanoparticles coated on the Fe_3O_4@SiO_2 nanorods could be modified by the interaction between Ag and Ni species through the so-

called ligand and strain effects,[36,37] which may also benefit the optimization of the catalytic performance. The detailed mechanism should be explored further.

The recyclability of the Fe_3O_4@SiO_2@Ag@Ni trepang-like nanocomposites is shown in Fig. 10. It can be seen that the nanocomposites show excellent catalytic efficiency even after six cycles without any significant loss of activity, indicating that the catalysts exhibit good reusability.

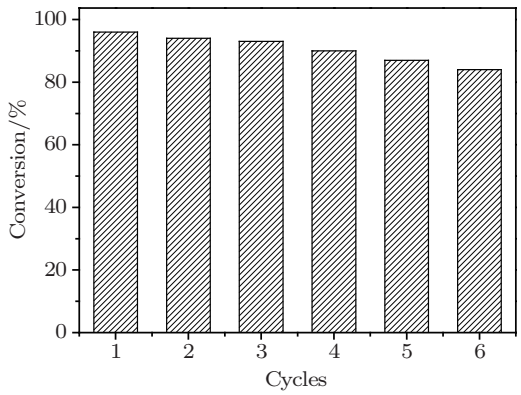


Fig. 10. Recycling of Fe_3O_4@SiO_2@Ag@Ni trepang-like nanocomposites for the degradation of RhB by $NaBH_4$.

4. Conclusions

In this work, a simple step-by-step method of synthesizing the Fe_3O_4@SiO_2@Ag@Ni trepang-like nanocomposites is developed. The as-prepared Fe_3O_4@SiO_2@Ag@Ni trepang-like nanocomposites exhibit an enhanced catalytic property for the degradation of RhB compared with monometallic Fe_3O_4@SiO_2@Ag nanorods. This catalyst could be easily collected from the catalytic system and retains high-efficiency even after six cycles of operation, which shows a great application potential for dealing with environmental issues.

References

[1] Liu S, Chen G Y, Prasad P N and Swihart M T 2011 *Chem. Mater.* **23** 4098
[2] Li P J, Chen K, Chen Y F, Wang Z G, Hao X, Liu J B, He J R and Zhang W L 2012 *Chin. Phys. B* **21** 118101
[3] Peng L, Mei Y, Chen S F, Zhang Y P, Hao J Y, Deng L L, and Huang W 2015 *Chin. Phys. B* **24** 115202
[4] Zhang Z, Liu Q and Qi Z M 2013 *Acta Phys. Sin.* **62** 060703 (in Chinese)
[5] Shen Z R, Matsuki Y, Higashimine K, Miyake M and Shimoda T 2012 *Chem. Lett.* **41** 644
[6] Zhang Q F, Large N, Nordlander P and Wang H 2014 *J. Phys. Chem. Lett.* **5** 370
[7] Fang Q L, Cheng Q, Xu H J and Xuan S H 2014 *Dalton Trans.* **43** 2588
[8] Hu H B, Wang Z H, Pan L, Zhao S P and Zhu S Y 2010 *J. Phys. Chem. C* **114** 7738
[9] Zhang Y L, Yan W W, Sun Z M, Li X C and Gao J P 2014 *RSC Adv.* **4** 38040
[10] Dhanda R and Kidwai M 2015 *J. Mater. Chem. A* **3** 19563
[11] Zhang S H, Gai S L, He F, Dai Y L, Gao P, Li L, Chen Y J and Yang P P 2014 *Nanoscale* **6** 7025
[12] Xu D, Liu Z, Yang H, Yang Q, Zhang J, Fang J, Zou S and Sun K 2009 *Angew. Chem. Int. Ed.* **48** 4217
[13] Chen G Z, Desinan S, Nechache R, Rosei R, Rosei F and Ma D L 2011 *Chem. Commun.* **47** 6308
[14] Krishna R, Fernandes D M, Dias C, Ventura J, Ramana E V, Freire C and Titus E 2015 *Int. J. Hydrogen Energy* **40** 4996
[15] Lin Y Y, Qiao Y, Wang Y J, Yan Y and Huang J B 2012 *J. Mater Chem.* **22** 18314
[16] Ai L H, Yue H T and Jiang J 2012 *J. Mater. Chem.* **22** 23447
[17] Tang S C, Vongehr S, Zheng Z, Liu H J and Meng X K 2010 *J. Phys. Chem. C* **114** 18338
[18] Zheng J M, Dong Y L, Wang W F, Ma Y H, Hu J, Chen X J and Chen X G 2013 *Nanoscale* **5** 4894
[19] Yue C, Yuan Q, Li Y J, Tu J C, Zhao L, Li N and Li X T 2012 *J. Colloid Interface Sci.* **383** 96
[20] Rathore P S, Patidar R and Thakore S 2014 *RSC Adv.* **4** 41111
[21] Bayat A, Fard M S, Ehyaei N and Hashemi M M 2015 *RSC Adv.* **5** 22503
[22] Yun G, Hassan Z, Lee J, Kim J, Lee N S, Kim N H, Baek K, Hwang I, Park C G and Kim K 2014 *Angew. Chem. Int. Ed.* **53** 6414
[23] Zhang Z W, Zhou Y M, Zhang Y W, Zhou S J, Xiang S M, Sheng X L and Jiang P 2015 *J. Mater. Chem. A* **3** 4642
[24] Li X Z, Wu K L, Ye Y and Wei X W 2014 *Cryst. Eng. Commun.* **16** 4406
[25] Zhang S H, Gai S L, He F, Ding S J, Li L and Yang P P 2014 *Nanoscale* **6** 11181
[26] Mao Y, Jiang W Q, Xuan S H, Fang Q L, Leung K C F, Ong B S, Wang S and Gong X L 2015 *Dalton Trans.* **44** 9538
[27] Jia C J, Sun L D, Yan Z G, You L P, Luo F, Han X D, Pang Y C, Zhang Z and Yan C H 2005 *Angew. Chem. Int. Ed.* **44** 4328
[28] Park J Y, Choi E S, Baek M J and Lee J H 2009 *Mater. Lett.* **63** 379
[29] Jiang H L, Akita T and Xu Q 2011 *Chem. Commun.* **47** 10999
[30] An Q, Zhang P, Li J M, Ma W F, Guo J, Hu J and Wang C C 2012 *Nanoscale* **4** 5210
[31] Chi Y, Yuan Q, Li Y J, Tu J C, Zhao L, Li N and Li X T 2012 *J. Colloid Int. Sci.* **383** 96
[32] Adeyeye A O, Bland J A C, Daboo C and Hasko D G 1997 *Phys. Rev. B* **56** 3265
[33] Ai L H, Yue H T and Jiang J 2012 *J. Mater. Chem.* **22** 23447
[34] Zhang Y, Zhu P L, Chen L, Li G, Zhou F R, Lu D Q, Sun R, Zhou F and Wong C P 2014 *J. Mater. Chem. A* **2** 11966
[35] Mao Y, Jiang W Q, Xuan S H, Fang Q L, Leung K C F, Ong B S, Wang S and Gong X L 2015 *Dalton Trans.* **44** 9538
[36] Kitchin J R, Norskov J K, Barteau M A and Chen J G 2004 *Phys. Rev. Lett.* **93** 156801
[37] Wang L M, Bai J, Lechtken A, Huang W, Schooss D, Kappes M M, Zeng X C and Wang L S 2009 *Phys. Rev. B* **79** 033413